

New structural and magnetic aspects of the nanotube system $\text{Na}_{2-x}\text{V}_3\text{O}_7$

O. Zaharko*, J. L. Gavilano, Th. Strassle

Laboratory for Neutron Scattering, ETH Zurich & Paul Scherrer Institut, CH-5232 Villigen, Switzerland

C. F. Miclea

Max-Planck-Institute for Chemical Physics of Solids (MPCPS), D-01187 Dresden, Germany

A. C. Mota

Laboratory for Solid State Physics, ETH-Honggerberg, CH-8093 Zurich, Switzerland and
Max-Planck-Institute for Chemical Physics of Solids (MPCPS), D-01187 Dresden, Germany

Y. Filinchuk, D. Chernyshov

Swiss-Norwegian Beam lines, ESRF, F-38042 Grenoble Cedex 9, France

P. P. Deen

Institut Laue-Langevin, 156X, F-38042 Grenoble Cedex 9, France

B. Rahaman, T. Saha-Dasgupta

S.N. Bose National Centre for Basic Sciences, JD Block,
Sector 3, Salt Lake City, Kolkata 700098, India

R. Valent

Institute of Theoretical Physics, University of Frankfurt, D-60438 Frankfurt, Germany

Y. Matsushita, A. Donni, H. Kitazawa

National Institute for Materials Science (NIMS), Tsukuba, Ibaraki 305-0047, Japan
(dated: February 20, 2024)

We present new experimental results of low temperature x-ray synchrotron diffraction, neutron scattering and very low temperature (mK-range) bulk measurements on the nanotube system $\text{Na}_2\text{V}_3\text{O}_7$. The crystal structure determined from our data is similar to the previously proposed model (P. Millet et al. J. Solid State Chem. 147, 676 (1999)), but also deviates from it in significant details. The structure comprises nanotubes along the c-axis formed by stacking units of two V-rings buckled in the ab-plane. The space group is $P\bar{3}$ and the composition is nonstoichiometric, $\text{Na}_{2-x}\text{V}_3\text{O}_7$, $x=0.17$. The thermal evolution of the lattice parameters reveals anisotropic lattice compression on cooling. Neutron scattering experiments monitor a very weak magnetic signal at energies from -20 to 9 meV. New magnetic susceptibility, specific heat measurements and decay of remanent magnetization in the 30 mK - 300 mK range reveal that the previously observed transition at 76 mK is spin-glass like with no long-range order. Presented experimental observations do not support models of isolated clusters, but are compatible with a model of odd-legged $S=1/2$ spin tubes possibly segmented into fragments with different lengths.

PACS numbers: 61.66.-f, 73.22.-f, 75.25.+z, 75.50.Lk

I. INTRODUCTION

The perspectives to create magnetic and electronic devices on the atomic scale motivates nowadays research on spin clusters, chains, ladders and other geometrical spin arrangements. Systems that accommodate such low-dimensional spin arrangements in a periodic fashion, i.e. on a lattice, are of particular interest. This is because their properties arising from individual objects and from the whole assembly can be probed by experimental and theoretical techniques developed for crystalline solids. One of the rare realizations of a crystalline system formed by nanotubes with periodic arrangement is $\text{Na}_2\text{V}_3\text{O}_7$, a compound first synthesized by Millet et al.¹. The struc-

ture is formed by VO_5 square pyramids connected via edges and apices (Fig. 1a). There are four inequivalent sodium sites. One Na site is located in the middle of the nanotube and the other three around the nanotubes. Buckled rings formed by nine V atoms (only three sites are inequivalent) have two different orientations forming slices A and B (Fig. 1b). The nanotube is formed by an -A-B-A-B- arrangement along the c-axis. Extensive experimental investigations employing specific heat, ac susceptibility and ^{23}Na nuclear magnetic resonance by Gavilano et al.^{2,3} revealed puzzling magnetic properties. Those results implied a gradual reduction of the number of V^{4+} $S=1/2$ magnetic moments, which may be due to the formation of dimers with most of them

in a singlet-spin and a small fraction with a triplet-spin ground state. Presence of a wide range of distributions of singlet-triplet energy gaps of dimerized V moments was claimed. The total gap distribution consists at least of three groups. Two of them, relatively narrow, are centered at 1 and 10 K and involve only 1/9 of vanadium moments. The third group, that corresponds to the 8/9 part of V moments, is very broad and this leads to a wide range of spin couplings. Additionally at very low temperatures, 86 mK, a phase transition was observed in the temperature dependence of the ac-magnetic susceptibility $\chi_{ac}(T)$. It was interpreted as a proximity to a quantum critical point at zero field.

Several theoretical calculations of the electronic structure and exchange interactions in $\text{Na}_2\text{V}_3\text{O}_7$ delivered conflicting results. A spin dimer analysis by Whangbo and Ko⁴ lead to the conclusion that $\text{Na}_2\text{V}_3\text{O}_7$ could be described by six mutually intersecting helical chains. A single helical chain has a spin gap and it is a good approximation for magnetic properties of the whole system. This is not supported by experimental results. The ab initio Density Functional Theory (DFT) calculations by Saha-Dasgupta et al.⁵, used the N-th order multi-orbital (NMO) based downfolding method to obtain a tight-binding Hamiltonian for V-3d_{xy} orbitals. Their microscopically derived hopping integrals resulted in antiferromagnetic (AF, $J < 0$) intra-ring exchange integrals dominating the inter-ring ones. This lead to the description of the system as weakly coupled nine-site rings with $J_1 = -200$ K and $J_2 = -140$ K intra-ring couplings. Mazurenko et al.⁶ performed DFT calculations with the local density approximation (LDA)+U approach and suggested that due to the strong hybridization between filled and vacant 3d vanadium orbitals the exchange interaction between V ions is dominated by strong ferromagnetic (F) inter-ring contributions, while the intra-ring exchange interactions are mainly antiferromagnetic. Their conclusion is that the resulting Heisenberg model is strongly frustrated and there is no simple way to predict the properties of the system.

The main goal of our paper is to provide, by characterizing static and dynamic, nuclear and magnetic, microscopic and macroscopic responses, a solid experimental background necessary to derive a correct model of the magnetic exchange in $\text{Na}_2\text{V}_3\text{O}_7$.

II. EXPERIMENTAL DETAILS

The $\text{Na}_2\text{V}_3\text{O}_7$ polycrystalline samples used in this study have been prepared by a solid-state reaction method using $\text{Na}_4\text{V}_2\text{O}_7$, V_2O_3 and V_2O_5 as described by Niitaka et al.⁷. The precursor $\text{Na}_4\text{V}_2\text{O}_7$ was synthesised from a mixture of NaCO_3 and V_2O_5 with a stoichiometric ratio, on a gold sheet at 873 K under air, and kept at 473 K before use. V_2O_3 was reduced from V_2O_5 by 7% H_2 + 93% Ar mixture gas. Under dry- and pure Ar atmosphere, the stoichiometric amount of

$\text{Na}_4\text{V}_2\text{O}_7 + \text{V}_2\text{O}_3 + \text{V}_2\text{O}_5$ was well mixed, and pressed into pellets. The pellets were wrapped in gold foils, and loaded into a fused silica tube. The tube was subsequently sealed under vacuum and heated in a furnace at 978 K for a week. The product was checked as pure $\text{Na}_2\text{V}_3\text{O}_7$ by x-ray powder diffraction⁸.

Analysis of the crystal structure and its evolution with temperature was studied by x-ray single crystal and powder diffraction. A black ber-like single crystal (10x10x700 μm) was extracted from the polycrystalline sample. X-ray diffraction studies have been performed at the BM 01A Swiss-Norwegian Beam line (SNBL) of ESRF, France, at a wavelength of 0.722870 Å, and at the Material Science Beam line (MSB) of SLS, Paul Scherrer Institute, Switzerland, with $\lambda = 0.620967$ Å. The crystal structure has been determined from a single crystal at SNBL at three different temperatures, 200 K, 80 K and 16 K, using an image-plate area detector MAR 345 and N_2 or He flow cryostats to reach low temperatures. 180 deg $^\circ$ oscillation images with an increment of 1 deg were collected with 1 min of exposure and the crystal-to-detector distance of 180 mm (see Table I). The quality of the data at 16 K is lower than at 80 K and 200 K due to a lower resolution obtained with the complex low-temperature experimental setup. The data were corrected for the Lorentz-polarisation factor and for absorption. For the structure solution and refinements the programs SHELXS and SHELXL⁹ were used.

Powder x-ray patterns were collected in a 0.5 mm quartz capillary at temperatures between 80 K – 470 K with the same setup used for the single crystal measurements. The experiment was performed on heating, with a heating rate of 120 K/h. One exposure lasted 30 s and the capillary was rotated 30 deg/exposure for better powder average. For patterns recorded in the temperature range of 14 K – 130 K a Janis He cryostat at MSB and a microstrip detector were used with 30 s exposure. Structure refinements were performed using the Rietveld technique implemented in the Fullprof program¹⁰.

Magnetic excitations and lattice vibrations were investigated on a 10 g polycrystalline sample. Inelastic neutron scattering measurements were performed on the neutron time-of-flight (TOF) spectrometer FOCUS at SINQ, PSI, Switzerland, at 1.5 K and 120 K. Three setups were exploited ($\lambda = 5.75, 4.85$ and 1.7 Å) to access energy-transfer ranges below 0.9, 2 and 20 meV, respectively, with optimal resolution. Contributions from an empty Al sample holder were measured and subtracted.

A powder neutron diffraction experiment with full three-directional (XYZ) neutron polarisation analysis was performed on the D7 instrument¹¹ at the Institute Laue-Langevin, France. The incident neutron wavelength 3.1 Å was selected using a pyrolytic graphite monochromator. Polarisation of the incident and analysis of the scattered beam were performed using polarising mirrors. Helmholtz coils enabled rotation of the incident neutron spins along three mutually perpen-

dicular directions. The efficiency of the 132 detectors of D7 was determined using a standard vanadium sample, while the polarisation efficiency was determined using a quartz sample with entirely non-spin flip scattering. The measurements were performed at 1.9, 120 K (each 60 h) and 300 K (2 h). Our experimental setup allowed us to measure the response of the sample within the wave vector range $0.5 < Q < 4 \text{ \AA}^{-1}$ and to integrate the signal over the energy interval $-1, 9 \text{ meV}$. The scattering from the sample was brought to the absolute scale using vanadium normalization. Absorption of the vanadium and the sample was taken into account. A powder non-polarized neutron diffraction experiment in the mK range was performed on DMC at SINQ, PSI, Switzerland, using a wavelength of $\lambda = 2.457 \text{ \AA}$. The sample was mounted into the dilution insert of an ILL orange cryostat and two diffraction patterns, at 40 mK and 1 K, were collected.

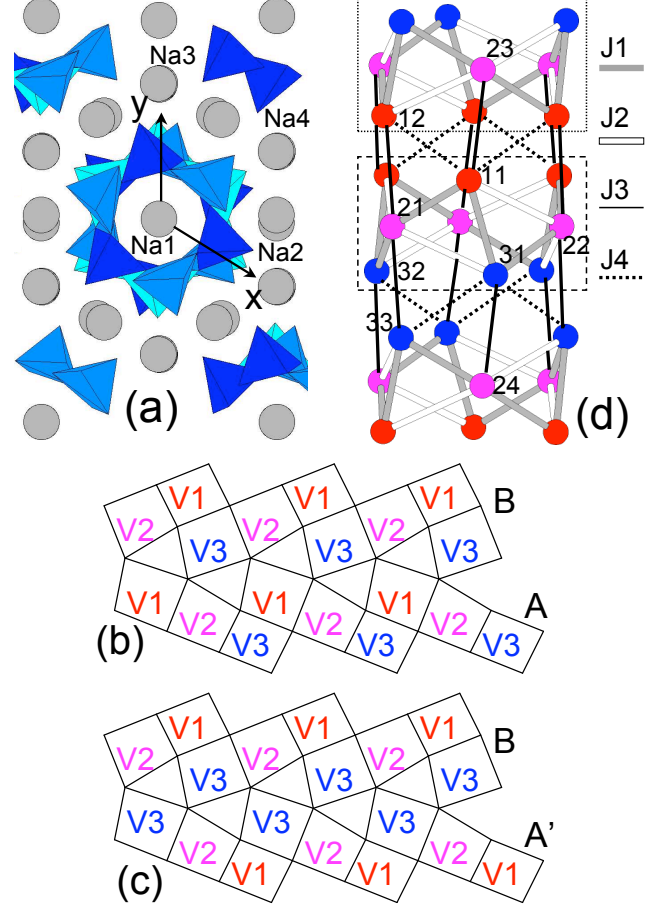
Measurements of the susceptibility on a polycrystalline sample were done at MPICPIS, Dresden in the 30 mK – 3.5 K range in an impedance bridge using a SQUID as a null detector. In this arrangement, the amplitude of the ac field can be varied in fixed steps from 0.07 to 33 mOe and the frequency can be chosen from 4 different values between 16 and 160 Hz. The sample was placed inside the mixing chamber of a dilution refrigerator. The residual field in the cryostat was less than 20 mOe. Specific heat measurements were performed using a quasi-adiabatic method in the temperature range 60 mK – 4 K at four values of applied field 0, 0.25, 0.5 and 2 T. The decay of the remanent magnetization was measured at MPICPIS, Dresden. The sample was cooled in a field of 100 Oe from $T = 200 \text{ mK}$ to the desired temperature $T < T_f$. Note that 200 mK is well above the critical temperature $T_f = 86 \text{ mK}$ where a cusp in χ_{ac} occurs. After a waiting time of about 10 hours, the field was removed and the relaxation of the remanent magnetization was recorded with a flux counter for about 20000 – 70000 seconds. After these times, the sample was heated to 200 mK and the expelled flux was recorded in order to obtain the total value of the remanent magnetization $M_{rem} = M_0 - M_1$.

III. RESULTS

A. Temperature evolution of the crystal structure

In an attempt to understand the magnetic exchange in $\text{Na}_2\text{V}_3\text{O}_7$ we performed detailed structural investigations at low temperatures. The analysis of the 200 K x-ray single crystal diffraction data set suggested an apparent Laue symmetry $\bar{3}m$ with mirror planes situated along the $[100]$, $[010]$ and $[110]$ directions. No systematic absences of the space group $P31c$ reported by Millet et al.¹ were observed. The direct methods were tentatively used with the following probable space groups $P\bar{3}1m$,

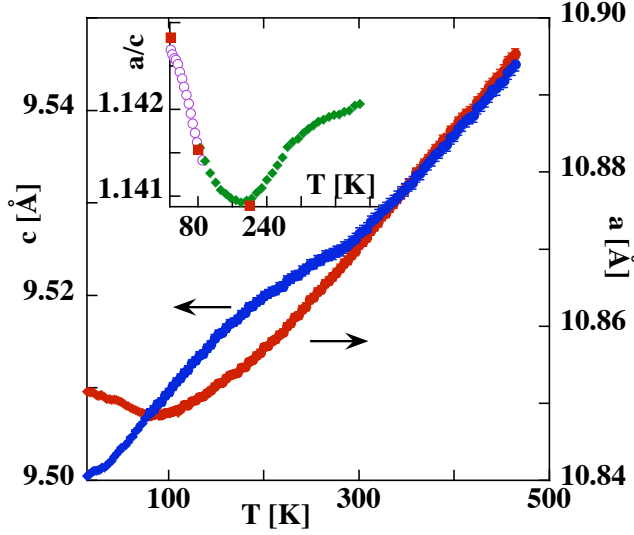
FIG. 1: a) $[001]$ projection of the $\text{Na}_2\text{V}_3\text{O}_7$ structure. Arrangement of V atoms forming buckled rings (slices A, B) within the nanotube b) in the model of Millet et al.¹ and c) in our model. The three sites of vanadium are denoted by V1 – red, V2 – pink, V3 – blue. Oxygen and sodium atoms are omitted for clarity. d) Four different families of exchange couplings J_1 (grey), J_2 (white), J_3 (black), J_4 (black dashed).



$P31m$ and $P312$, but no acceptable solution was found. Therefore, the presence of $f010g$ twinning of the crystal with $P3$ or $P\bar{3}$ symmetry has been considered. The centrosymmetric model presented in Table II with 50% of two twin domains explained well the apparent $\bar{3}1m$ symmetry. The R -values corresponding to the final refinements are presented in Table I. The anisotropic displacement parameters and occupancies of all atoms could be refined at 80 K and 200 K (see Table III). For the 16 K data set, due to its lower resolution, isotropic displacement parameters were used.

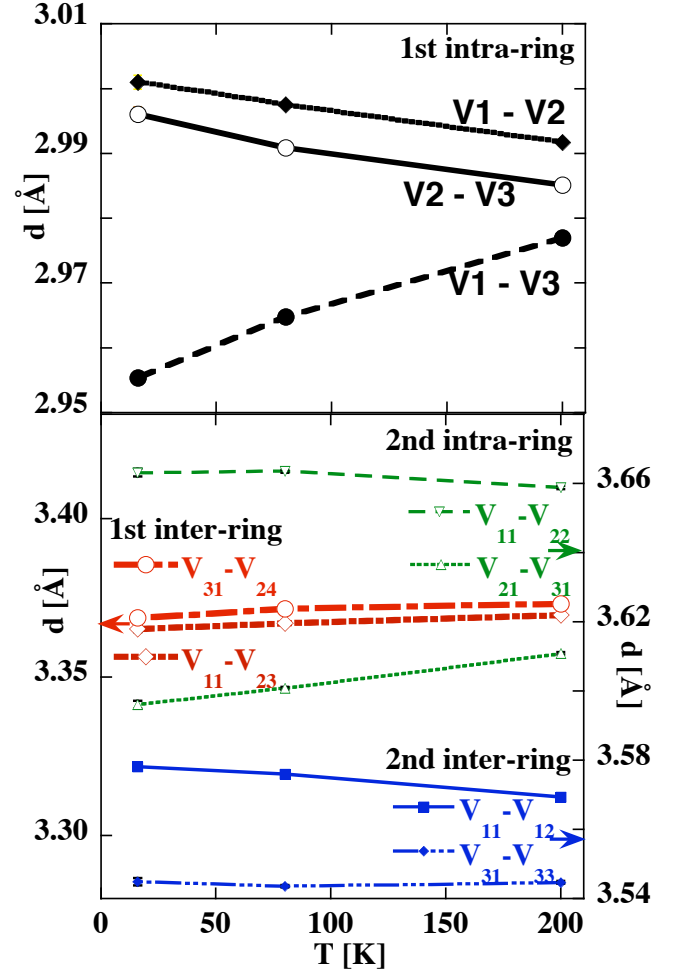
Single crystal data collected at three temperatures indicate no structural phase transition. The structure resulting from our analysis is very similar to the model proposed by Millet et al.¹ However, there are important differences. The arrangement of nine V atoms into the buckled ring (slice) B is the same as in the model of Millet (Figs. 1b and c). But due to the absence of the glide plane in the $P\bar{3}$ space group, the slice A' is oriented

FIG. 2: Thermal expansion of the lattice parameters a (red) and c (blue) from x-ray powder diffraction. Inset: The a/c ratio calculated from the SNBL (green), SLS (violet) powder patterns and SNBL (red) single crystal data.



di erently compared to A.W e identify the A'-B two-ring stacking unit as a structural building block of $\text{Na}_2\text{V}_3\text{O}_7$. A detailed structural investigation resulted in precise values of the V-V distances and V-O-V angles presented in Tables IV,V. Here a second index in the notation of V atoms is introduced to simplify the comparison of numerical and graphical presentations (see also Fig. 1d). Based on these values it is possible to distinguish four different families of effective exchange paths. They are: 1st and 2nd intra-ring and 1st and 2nd inter-ring ones. In a simplified model for the magnetic exchange in $\text{Na}_2\text{V}_3\text{O}_7$ each family may be represented by a single exchange coupling (J_1 - J_4 , see Fig. 1d). The 1st intra-ring exchange path is characterized by the average shortest V-V distance of 2.985 Å and the V-O-V angles of 99 deg. Thus it is the most important coupling. The 2nd intra-ring path has rather large V-V distances (3.63 Å) and V-O-V angles of 140 deg. The 2nd inter-ring path has smaller V-V distances (3.55 Å) and almost the same V-O-V angles of 132 deg. Therefore, based solely on the atomic arrangement, the 2nd intra-ring and 2nd inter-ring paths might be equally important. The 1st inter-ring path will certainly result in a 'separate' coupling as the V-V distance is 3.37 Å and the V-O-V angles are 119 deg. DFT calculations⁵ performed on the crystal structure proposed by Millet et al.¹ identify the 1st and 2nd intra-ring couplings as the most important ones. And, according to these calculations, the 2nd intra-ring and 2nd inter-ring couplings are significantly different due to the orientation of the V orbitals. As small differences in the atomic arrangement between our model and the model of Millet, can significantly change the strength

FIG. 3: Thermal evolution of the V-V distances calculated from single crystal x-ray diffraction at 200, 80 and 16 K. Top: 1st intra-ring distances, bottom: 2nd intra-ring (green), 1st (red) and 2nd (blue) inter-ring distances.



and even the sign of the magnetic exchange⁶, we revised the electronic structure of $\text{Na}_2\text{V}_3\text{O}_7$ performing new DFT calculations (see Section IV).

In the new model of crystal structure, within the vanadium-oxide nanotubes there are two inequivalent Na sites, 1(a) and 1(b). They are only partially occupied. This leads to a nonstoichiometric composition $\text{Na}_{2-x}\text{V}_3\text{O}_7$ with $x=0.17$. The requirement of neutrality of the crystal inquires that the missing positive charge is distributed on the neighboring atoms; either some amount of V^{5+} (up to 5.7%) or intermediate valence states should be present. These minority states, if localized on V, could serve as defects introducing randomness into the V-V exchange couplings.

The displacement parameters U of all atoms, including sodium, are small, almost isotropic (see Table III) and decrease with temperature lowering, as in conventional

materials. Therefore, the assumptions used to identify the low frequency phonon mode at 88 cm^{-1} as the Na rattling mode¹⁷ does not hold. Our Na^+ mean square displacement amplitude $\langle u^2 \rangle$ is approximately six times smaller than assumed by Choi et al.¹⁷ and therefore the characteristic frequency would be 174 cm^{-1} , which is incompatible with the observed hypothesized rattling mode at 88 cm^{-1} .

One more important outcome of our x-ray diffraction study is the temperature evolution of the lattice parameters a and c . Powder patterns reveal that the lattice compresses gradually on cooling (Fig. 2). This compression is very anisotropic, as visualized in the a/c ratio in the inset of Fig. 2. Whilst above 300 K the expansion coefficients α_a and α_c lie in the range of $10^{-6}/\text{K}$, which is typical for oxides; several anomalies in $\alpha(T)$ and $\alpha_c(T)$ are observed at lower temperatures. Near 300 K the decrease of c slows down, close to 100 K with decreasing temperature, $\alpha(T)$ starts to increase. Unfortunately we cannot supply microscopic details of all these changes, but we reckon that the changes near 100 K correlate with the anomaly observed in the ^{23}Na -NMR spin-lattice relaxation rate³ and the 88 cm^{-1} mode detected in optical measurements¹⁷.

The variation of the V-V distances and V-O-V angles obtained from single crystal refinements (Tables IV, V and Fig. 3) allows us to conclude that the dominant tendency is a reduction of the V-V distances and V-O-V angles having the largest projection along the tubes and an increase of those having a substantial xy-component.

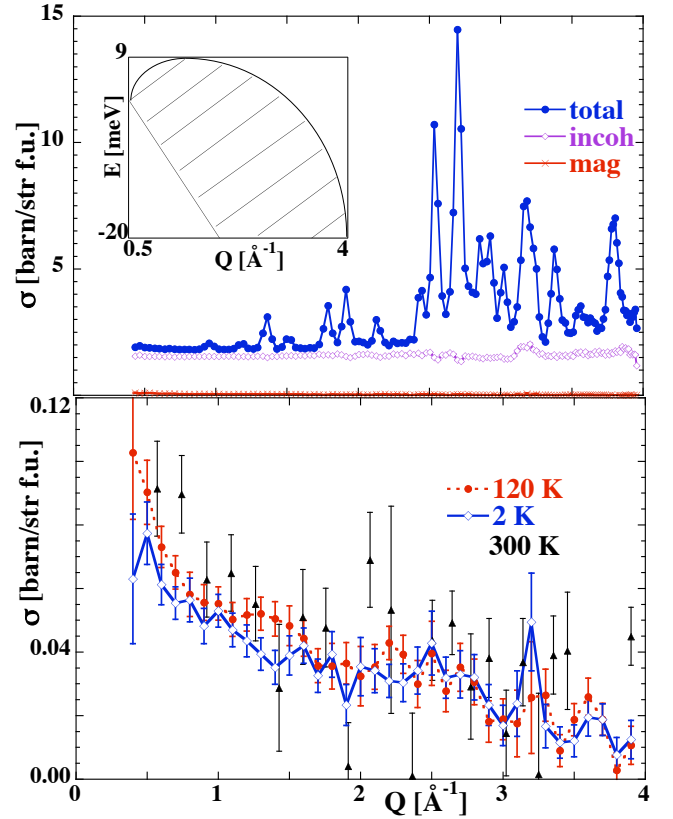
B. Neutron scattering: polarized diffraction and time-of-flight inelastic scattering

We performed neutron scattering experiments to obtain information on the static and dynamic magnetic correlation functions in $\text{Na}_{2-x}\text{V}_3\text{O}_7$. This system has significant incoherent scattering σ_{incoh} due to the presence of vanadium and sodium. σ_{incoh} is comparable to the magnetic scattering of V ($\sigma_{\text{incoh}} = 1.47 \text{ barn/str. f.u.}$, $\sigma_{\text{mag}} = 0.437 \text{ barn/str. f.u.}$), additionally absorption is significant. Therefore, a polarised neutron diffraction experiment was carried out on D7 to separate magnetic scattering from nuclear coherent, nuclear spin incoherent and background contributions. The paramagnetic scattering was obtained by averaging the contributions extracted from the spin-flip (SF) and non-spin-flip (NSF) partial cross sections¹³:

$$\begin{aligned} \frac{d^2 \sigma_{\text{mag}}}{d\Omega dE} &= 2 \left[\frac{d^2 \sigma_{\text{SF}}^x}{d\Omega dE} + \frac{d^2 \sigma_{\text{SF}}^y}{d\Omega dE} - 2 \frac{d^2 \sigma_{\text{SF}}^z}{d\Omega dE} \right] \\ \frac{d^2 \sigma_{\text{mag}}}{d\Omega dE} &= 2 \left[\frac{d^2 \sigma_{\text{NSF}}^x}{d\Omega dE} - \frac{d^2 \sigma_{\text{NSF}}^y}{d\Omega dE} + 2 \frac{d^2 \sigma_{\text{NSF}}^z}{d\Omega dE} \right] \quad (1) \end{aligned}$$

where z is perpendicular to the scattering plane. Fig. 4 (top) presents total, nuclear spin incoherent and magnetic signals from the sample. Apparently the mag-

FIG. 4: Top: total, nuclear spin incoherent and magnetic scattering at 120 K measured on D7 with $\lambda = 3.1 \text{ \AA}$. Inset: The (Q, E) window accessible during the experiment is shown by the dashed area. Bottom: Absolute magnetic scattering at $1.8, 120$ and 300 K .



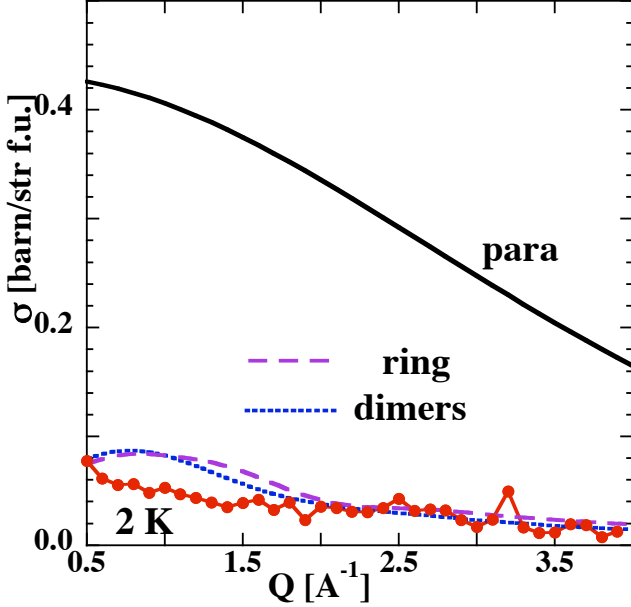
netic signal is tiny. The amount of magnetic scattering summed over the measured Q -range is only 13 % of the expected paramagnetic scattering of $\text{Na}_{2-x}\text{V}_3\text{O}_7$ formula unit (f.u.) in this Q -interval calculated as

$$\sigma_{\text{mag}} = \frac{2}{3} N S(S+1) (r_0)^2 f^2(Q); \quad (2)$$

where $\frac{2}{3}$ results from the powder average, $N = 3$ is the number of spin $S = 1/2 \text{ V}^{4+}$ ions per f.u., $(r_0) = -0.54 \cdot 10^{-12} \text{ cm}$ and $f(Q)$ is the magnetic form factor of V^{4+} . The weakness of the signal caused long counting times to obtain reasonable statistics in the diffraction mode, i.e. integrating over all energy window, and it was impossible to measure the (Q, E) distribution of the magnetic scattering in TOF mode of D7.

Fig. 4 (bottom) presents magnetic contributions at $1.8, 120$ and 300 K . The signals are almost equal and featureless within statistical errors. This leads to important conclusions. Firstly, the majority of magnetic intensity remains out of the integrated energy and momentum window of our experiment shown as an inset in Fig. 4 (top). At 1.8 K dominantly elastic and neutron energy loss events are measured, while at 120 K additionally the

FIG. 5: Comparison of the magnetic scattering at 2 K measured on D7 (red) and the calculated paramagnetic signal of V^{4+} (black solid), both in absolute scale. Calculated low-lying excitations of an isolated nine-member ring (violet dashed) and of an isolated dimer (blue dotted) are given in arbitrary units.

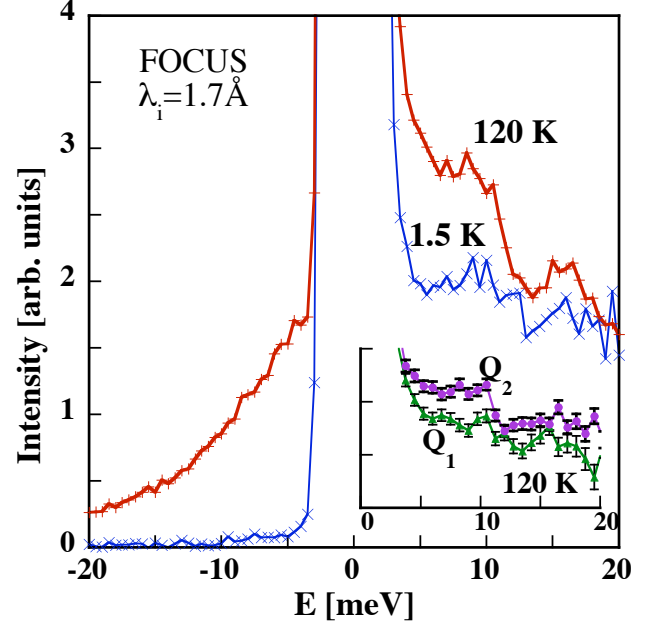


neutron energy gain side up to $2kT = 20$ meV is accessible. In both measurements the magnetic scattering is very weak and it only slightly increases from 1.8 to 120 K in the low Q range, which implies presence of high-energy states becoming populated at higher temperature. The total paramagnetic scattering is not recovered even at 300 K (Figs. 4, 5), therefore, most of the magnetic intensity is located at even higher energy transfers. Secondly, observation of weak magnetic intensity with no oscillation in the Q -dependence disputes the presence of isolated clusters. Any isolated magnetic cluster would have a characteristic oscillation in the Q -dependence, which arises due to the geometric $\frac{\sin(Q \cdot R)}{Q \cdot R}$ term in the neutron cross section¹⁴:

$$\frac{d^2_{\text{mag}}}{d\Omega^2} / f^2(Q) = \sum_{j < j^0}^n (j < S_j T_j T_{j^0} S^0 > j) + 2 \frac{\sin(Q \cdot R)}{Q \cdot R} < S_j T_j T_{j^0} S^0 > < S^0 T_j T_{j^0} S > \quad (3)$$

where $R = R_j - R_{j^0}$ is the distance between the V^{4+} ions i and j of the cluster, T_j -are irreducible tensor operators. Fig. 5 presents the expected Q -dependences for an isolated nine-member ring and an isolated dimer calculated using programs of Wille¹⁵. For the nine-member ring the Hamiltonian is $H = J_1 \sum_{i=1}^9 (S_i \cdot S_{i+1}) + J_2 \sum_{i,j} (S_i \cdot S_j)$ (for $i=2, j=4, 9$, for $i=5, j=3, 7$, for $i=8, j=1, 6$) and the two intra-ring antiferromagnetic exchange constants are $J_1 = -160$ K and $J_2 = -90$ K, the best estimate from our present susceptibility data (see Section V).

FIG. 6: INS spectra of $\text{Na}_{2-x}\text{V}_3\text{O}_7$ at 1.5 K (blue) and 120 K (red) measured on FOCUS with $\lambda_i = 1.7$ Å. The intensity has been integrated over the momentum transfer range $2.1 < Q < 5.7$ Å⁻¹. Inset: Q -dependence at 120 K for $2.6 < Q < 3.4$ Å⁻¹ (green) and $4.1 < Q < 4.9$ Å⁻¹ (magenta).



The geometric term is summed over the excitations between the 16 lowest cluster levels which could contribute to the integrated energy window of the D7 experiment and R 's correspond to the V - V intra-ring distances determined in this work. For the dimer the Hamiltonian is $H = J(S_1 \cdot S_2)$ with the antiferromagnetic exchange constant J chosen such that the spin singlet-triplet excitation lies in the energy window of the experiment, R is the average 1st intra-ring distance. None of the calculated Q -dependences is consistent with the measured one.

Yet, our observations are compatible with two following pictures: i) $\text{Na}_{2-x}\text{V}_3\text{O}_7$ is composed of complex objects, i.e. spin clusters with different sizes and exchange couplings, and the Q -dependence of each individual cluster is blurt out; ii) nine-member ring spin clusters are coupled into tubes, this leads to dispersion of excitations and to smearing of oscillations in the measured energy integrated $S(Q, \omega)$. An intermediate picture, nanotubes segmented into finite fragments with different length, also explains the observations.

Inelastic neutron scattering collected at two temperatures 1.5 and 120 K (Fig. 6) in the TOF mode on FOCUS is dominated by incoherent scattering. No distinct magnetic excitations have been observed up to 20 meV in agreement with the D7 results. The weak mode observed near 0 meV is most probably due to phonons since its intensity increases with Q and temperature (Fig. 6 inset). It is found close to the 88 cm⁻¹ mode observed by optical

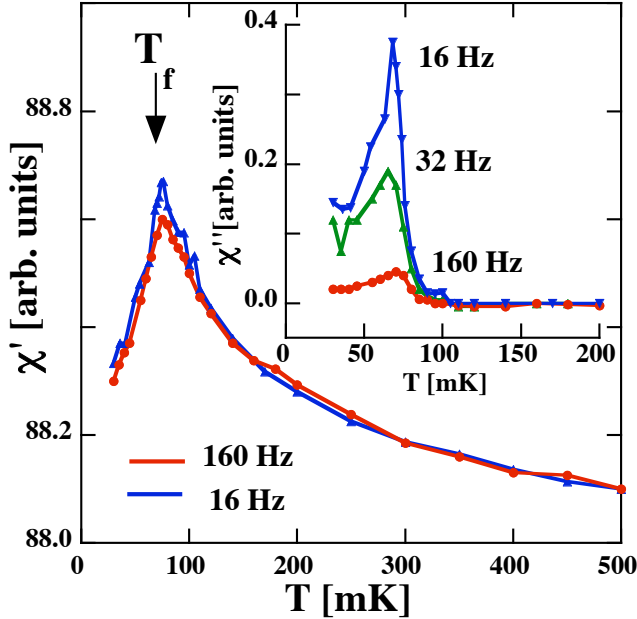
measurements¹⁷. Our observations, however, does not allow us to specify which atoms (V or Na) are involved in this mode.

C. Magnetic properties in the mK temperature range

1. ac-susceptibility and specific heat

We performed new experiments in the mK temperature range to characterize the previously found³ very low-temperature state of $\text{Na}_2\text{V}_3\text{O}_7$. First of all, our ac-

FIG. 7: Temperature and frequency dependence of real χ' and imaginary χ'' components of ac-susceptibility in mK temperature range.



susceptibility measurements confirm the sharp anomaly in $\chi(T)$ in the form of a "cusp". The temperature dependencies of both, the in-phase χ' and out-of-phase χ'' components display peaks near 76 mK (Fig. 7), which is slightly lower than the reported value³. Although χ' has only a very weak frequency dependence, the magnitude and shape of χ'' (Fig. 7 inset) are strongly frequency dependent. In particular, the temperature where the maximum of χ'' occurs decreases slightly with decreasing frequency. These observations hint for a slow dynamics of the V^{4+} moments reminiscent of spin-glass-like processes with a freezing temperature $T_f = 76$ mK.

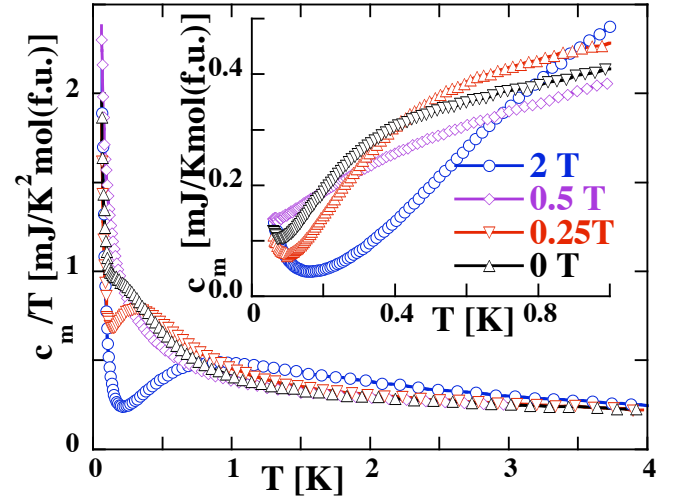
Although the anomaly in $\chi(T)$ at T_f signals a change in the magnetic properties of $\text{Na}_2\text{V}_3\text{O}_7$, the state below T_f is not long-range magnetically ordered. This is consistent with powder neutron diffraction. The patterns collected at 40 mK and 1 K were identical, no magnetic reflections

occurred at low temperature.

Fig. 8 inset displays the low-temperature part of the magnetic specific heat C_m obtained by subtracting the lattice contribution from the measured signal¹⁶. $C_m(T)$ shows no clear features near T_f . This important result shows that the number of degrees of freedom involved in the spin-freezing phenomenon must be rather small compared to the number of V^{4+} ions. The second important feature is a broad Schottky-like feature near 0.4 K, which shifts to higher temperatures with applied field. Approximately 1/13 of the magnetic entropy is associated with this feature. It is worth to recall that there is also a broad feature at 5 K, where at most 1/9 of the magnetic entropy is released as found previously³.

And finally, there is a strong upturn in $C_m = T$ with de-

FIG. 8: Magnetic part of the specific heat divided by temperature, $C_m = T$, versus T for different fields. Inset: C_m versus T below 1 K.



creasing temperature below 0.15 K (Fig. 8). This upturn is well represented by $C_N = T = D = T^3$. D is of the order of $2 \cdot 10^4$ to $4 \cdot 10^4$ (J (mole f.u. K)⁻¹) and C_N is only weakly field dependent. Paramagnetic impurities (i.e. only weakly- or non-interacting magnetic ions) cannot be the origin of this feature because their contribution would be strongly suppressed by a field of 2 T, contrary to the experimental observations. The impurities, however, could come from a nuclear contribution to the specific heat due to i) nuclear quadrupolar energy levels and ii) nuclear Zeeman levels.

First let's roughly estimate the contribution from nuclear quadrupolar energy levels. Nuclei with spin I and quadrupolar moment eQ exposed to static electric field gradients, where the largest component is denoted as eq , contribute to the specific heat (per mole of the considered nuclei)¹⁸: $C_N = D_Q - T^{-2}$, with

$$\frac{D_Q}{R} = \frac{1}{80} \frac{(2I+2)(2I+3)}{2I(2I-1)} \frac{e^2 q Q^2}{k_B} \quad (4)$$

R is the universal gas constant, k_B is the Boltzmann constant and e is the electron charge. The most promising candidates to provide a substantial contribution to the specific heat are the ^{51}V nuclei which have¹⁹ $I = 7/2$, a large $Q = 5.2 \cdot 10^{15} \text{ m}^2$ and low point symmetry. From Eq. 4 with $D_Q = 4 \cdot 10^4 \text{ (J mole fu. K}^{-1})$ it follows $eq \approx 4 \cdot 10^{23} \text{ V/m}$. This value is about two orders of magnitude too large compared with experimental NMR studies of other V compounds²⁰. Therefore, the nuclear quadrupolar levels seem to be improbable reason of our observed results.

Second we consider nuclear Zeeman levels. Assume a fraction f of magnetic V moments, which are at/near freezing. The direct contribution from these moments was already discarded previously. However, an indirect contribution via the hyperfine field coupling to the nuclei should also be taken into account. The nuclei are influenced by the on-site moment via the core polarization. This would result in a local field of the order of 100 T (per B of on-site V moment)²⁰. The magnetic nuclear contribution to C_N is $C_N = D_Z = T^2$, with

$$\frac{D_Z}{R} = 3f \frac{(2I + 2)}{6I} \frac{N \sim IH_1}{k_B} : \quad (5)$$

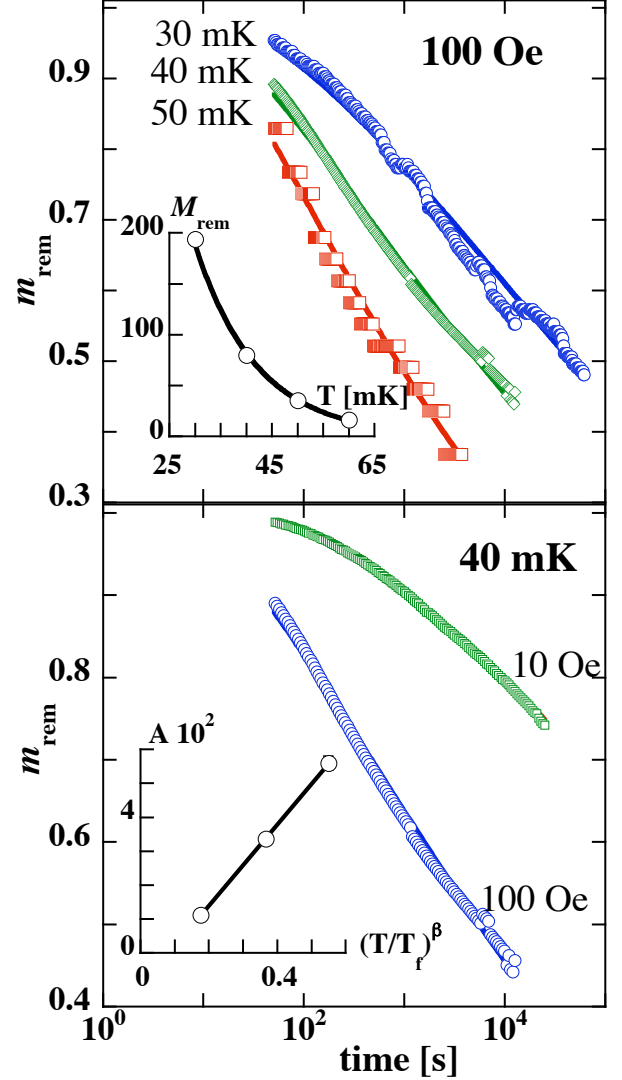
This takes into account that there are 3 V ions per formula unit and assumes that only a fraction f of V ions are magnetic. $N = 7.045 \cdot 10^7 \text{ (rad (sT)}^{-1}\text{T)}^{19}$ is the nuclear gyromagnetic ratio of ^{51}V and H_1 is the local magnetic field. With $I = 7/2$ and $H_1 = 100 \text{ T}$ this leads to $f = 0.001$. We conclude that a tiny amount of "frozen" V moments acting on their nuclei via the hyperfine field would explain the observed $C_N(T)$ at low temperatures.

2. Decay of remanent magnetization

The dynamics of the V moments on a long-time scale at temperatures below T_f was probed by measuring the decay of the remanent magnetization $M_{\text{rem}} = M_0 - M_1$. We recall that in these experiments the sample is cooled to a given temperature $T < T_f$ in a fixed external magnetic field $H = 100 \text{ Oe}$. After a waiting time of about 10h, H is turned to zero at $t = 0$ and the time evolution of the magnetization M_t is monitored, keeping T fixed. The decay of $M_t - M_1$ does not follow a simple functional form and is extremely slow (Fig. 9) indicative of a spin-glass like behaviour. Characteristic time scales are of the order of 10^4 sec , which we define as the time where $M_t - M_1$ reaches a fraction $1/e$ of its initial value. As shown in the inset of Fig. 9 top, M_{rem} grows exponentially with decreasing temperature.

For different spin-glass systems the magnetization decays follow different functional forms. The functional form of $M_t - M_1$ is determined by the distribution of barriers that the system should overcome to reach the

FIG. 9: Temperature and frequency dependence of the normalized remanent magnetization $m_{\text{rem}} = \frac{M_t - M_1}{M_0 - M_1}$. Top: the same cooling field of 100 Oe has been used and measurement performed at different temperatures. Inset: M_{rem} [arb. units] versus T . Bottom: different cooling fields of 100 and 10 Oe have been used and measurement performed at 40 mK. Inset: A versus T .



equilibrium. Our data are well characterized by the so-called "enhanced power law" given by^{22,23}:

$$m_{\text{rem}} = \frac{M_t - M_1}{M_0 - M_1} = \exp f A [\ln(t)]^g \quad (6)$$

This functional form is rather general, and it reduces, for instance, to a "logarithmic" type-decay for the particular case of $f = 1$, $A \ll 1$ and t not too large. The underlying model assumes that as temperature decreases there is a spontaneous formation of clusters of correlated spins with non-zero total spin, which grow randomly and independently from each other leaving a "void" of individual spins in between. To reach

the thermal equilibrium a spin-reorientation of these clusters must occur, and barriers, which depend on the cluster volume V , must be overcome to reach thermal equilibrium. This yields a hierarchy of relaxation times and results in the enhanced power-law for the decay of the magnetization.

The above form of the decay does not depend on the mechanism that drives the relaxation, which may be either quantum tunneling (QT) or thermal activation (TA). In addition the three parameters describing relaxation A , τ , and ω do not independently vary with temperature. For instance, the attempt frequency ω may be assumed T independent. In case of quantum tunneling the parameters A and τ are also T independent, resulting in a temperature independent relaxation. This is clearly not the case in our experiments (Fig. 9). In the case of thermal activation ω is T independent, but A and τ are correlated; namely, $A \propto (T - T_f)^{23}$.

To a good approximation A versus T deduced from our fits (inset of Fig. 9 bottom) is a straight line. Therefore, our data suggest a classical type of spin-glass phenomena driven by thermal activation, even at the lowest temperatures.

Our observations are not consistent with the 'superparamagnetic' picture describing the Mn_{12}^{24} , V_{15}^{25} , Fe_{13}^{26} cluster systems. There, a well defined and unique magnetic barrier leads to a single relaxation time resulting in a single exponential decay.

IV. AB INITIO DFT CALCULATIONS

We have performed ab initio DFT calculations for the new crystal structure determined in this work (see Table II) and applied the NMT0-based downfolding method in order to obtain the effective vanadium-vanadium hopping matrix elements. We considered a crystal structure with 100% occupation of the Na positions. The analysis of the Na density of states (DOS) contribution near the Fermi level shows that the effect of Na is almost negligible concerning the V hybridizations, and therefore significant changes of the electronic structure are not to be expected by reducing the Na content in the calculations. Variations in the hopping integral determination between the crystal structure proposed by Millet et al.^{1,5} and the present one are only observed in (i) the 1st and 2nd intra-ring hopping parameters which are now almost identical, enforcing the frustration effects in this system, and (ii) the inter-ring hopping parameters are slightly larger than those obtained previously, but remain still weaker than the intra-ring hopping parameters. The analysis of the orbital orientation in the 2nd intra-ring and 2nd inter-ring paths shows that, even though distances and angles are similar for both cases, the inter-ring hybridizations are of dd type explaining the weakness of the hopping integral in contrast to the mixed dd nature of the intra-ring orbital hybridization. Still, the exchange

coupling constants between V_i and V_j , J_{ij} are very sensitive to ferromagnetic J_{ij}^{FM} and antiferromagnetic J_{ij}^{AFM} contributions, $J_{ij} = J_{ij}^{FM} + J_{ij}^{AFM}$. Calculation of J_{ij}^{AFM} due to the hybridization of $V d_{xy}$ orbitals, shows that the antiferromagnetic intra-ring exchange interactions are a factor of four larger than the antiferromagnetic inter-ring exchange interactions. The ferromagnetic contributions J_{ij}^{FM} , which can be estimated following the Kugel-Khomskii model^{6,27} are, on the contrary, of the same order of magnitude for intra- and inter-ring couplings, so that in conclusion, the intra-ring interactions J_{intra} are dominantly antiferromagnetic, while the inter-ring interactions J_{inter} have important ferromagnetic components as pointed out also in Ref. 6.

V. SUMMARY

We presented new experimental results which allow to advance the understanding of the puzzling properties of the nanotube system $Na_{2-x}V_3O_7$. Revisited crystal structure belongs to the $P\bar{3}$ space group, while the apparent $\bar{3}m$ symmetry is due to twinning. The bucked ring of nine V atoms, is the same as in the model of Millet et al.¹, but the orientation of rings in the nanotube is different. The A'-B two-ring stacking unit is the basic structural building block.

We found off-stoichiometry in the sodium composition that might introduce randomness into the exchange couplings or presence of up to 5.7% of V^{5+} defects. The lattice compression with decreasing temperature is very anisotropic, with several anomalous points that correlate with previous NMR and optical measurements. With decreasing temperature the dominant tendency is a reduction of distances directed mostly along the tube and an increase of those having substantial xy -component. No experimental support of a structural transition, spin dimerization and Na rattling was found. In the neutron scattering experiments we observed a weak magnetic signal in the energy window of our experiment from -20 to 9 meV, implying that the majority of magnetic excitations are located above 20 meV. This is consistent with specific heat data, which indicate that at most 1/9 of the total magnetic entropy is released below 20 K, and with the susceptibility data, which monitor one order of magnitude moment reduction below 100 K. The magnetic scattering does not have a pronounced Q -dependence expected for spin clusters and, therefore, does not support the models of dimer formation or presence of isolated nine-member rings. The data might be explained, however, by the existence of clusters with different size and couplings or/and significant inter-cluster couplings smearing out oscillations in $S(Q; \omega)$. We note, however, that these scenarios leave unexplained the prominent peak in the temperature dependence of the spin-lattice relaxation rate around 100 K³. That peak was used as part of the evidence that spin dimerization may occur in that

temperature range. But our present findings show that it is improbable.

Our present and previous experimental observations allow us to suggest the following picture: The $\text{Na}_{2-x}\text{V}_3\text{O}_7$ system consists of segmented $S=1/2$ spin nanotubes with strong AF intra-ring but also significant inter-ring couplings. We speculate that segmentation happens due to the defects occurring because of the deviations from ideal stoichiometry.

Though the dominant feature of susceptibility, the upturn at 100 K, can be well reproduced by an isolated nine-member ring with $J_1 = -160$ K and $J_2 = -90$ K (Fig. 10), other experimental observations on $\text{Na}_{2-x}\text{V}_3\text{O}_7$, i.e. neutron magnetic scattering, object a picture of isolated nine-member rings and require the presence of inter-ring couplings or more complex spin objects. The susceptibility is dominated by strong intra-cluster couplings and is not a sensitive measure of the weaker inter-cluster couplings. A similar situation happens in coupled systems of triangles²⁹ and tetrahedra^{30,31}.

ab initio calculations point to larger intra-ring than inter-ring hopping integrals. The evaluation of the exchange integrals suggest strong antiferromagnetic inter-ring interactions and moderate intra-ring interactions mostly of ferromagnetic nature.

As there is a small magnetic moment at low T , we infer that $\text{Na}_{2-x}\text{V}_3\text{O}_7$ belongs to the class of odd-legged $S=1/2$ spin tubes with a gapless excitation spectrum and main spectral weight located at high T . As shown by Luscher et al.³² frustrated inter-ring couplings might lead to the absence of a spin gap, which otherwise should be present in odd-legged tubes. A single crystal inelastic neutron scattering experiment is needed to verify our hypothesis, to obtain the inter-ring couplings and to explain the low-temperature features at 0.4 and 5 K in specific heat.

The basic question, whether the ground state is magnetic or non-magnetic, still cannot be answered unambiguously. The origin of the 76 mK anomaly and of the observed slow dynamics in the mK range is not immediately evident. Our data strongly suggest a classical "spin-freezing" type phenomenon. But, given the small amount of spins involved (of the order of 0.1%) it is difficult to ascertain whether this behaviour is intrinsic to the ideal nanotube or it is induced by segmentation of nanotubes.

VII. ACKNOWLEDGMENTS

The work was partially performed at SINQ, Paul Scherrer Institute, Villigen, Switzerland, at the ILL re-

actor, and at the Swiss-Norwegian Beam lines, ESRF, Grenoble, France. The work at MPICPFS was carried out within the DFG project MI171/1-1. The work at ITP Frankfurt was carried out within the DFG project

FIG. 10: Temperature dependence of inverse susceptibility obtained from our experiment (symbols) and calculated (solid line) for an isolated nine-member ring with $J_1 = -160$ K and $J_2 = -90$ K. Inset: energy distribution of 512 levels of the ring as a function of the total spin S . Calculations were performed using the alps program³³.

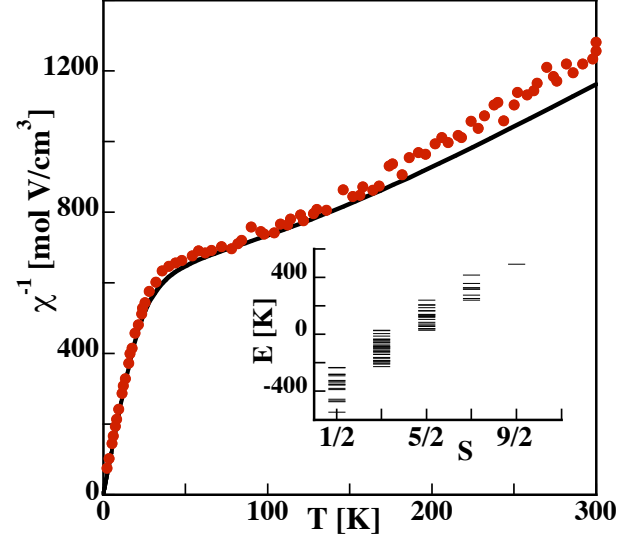


TABLE I: Details of single crystal x-ray diffraction data collection and structure refinement for $\text{Na}_{2-x}\text{V}_3\text{O}_7$ at three different temperatures.

T (K)	200	80	16
a (Å)	10.8827(5)	10.8747(3)	10.8748(1)
c (Å)	9.5506(2)	9.5382(1)	9.5275(2)
V (Å ³)	979.57	976.86	975.77
2 _{max} (deg)	59.75	59.81	42.99
R _{int} %	0.0182	0.0153	0.0423
Re. collected	10485	1744	689
Re. unique	1744	1744	689
restraints	0	0	18
refined parameters	113	113	69
R, wR (I ² (I)) %	1.24, 3.99	1.23, 3.78	1.91, 5.16
Goodness of fit	1.23	1.15	1.17
largest diff. peak max/min in and hole/e Å ⁻³	0.33/-0.32	0.38/-0.33	0.31/-0.27

SFB/TR49. We thank for the expert assistance by Dr. F. Gozzo, Swiss Light Source and Dr. L. Keller, SINQ, PSI.

* email: Oksana.Zaharko@psi.ch

¹ P. Millet, J. Y. Henry, F. M. M. J. Galy J. Solid State Chem.

TABLE II: Atomic coordinates xyz and isotropic displacement parameters U_{iso} (10\AA^2) in $\text{Na}_2\text{V}_3\text{O}_7$ at 200 K. The space group is $\bar{P}3$, $Z=6$, twin proportion is 49.90(9) and 50.10(9)%. The Na1 and Na2 sites are occupied only 45.3(11) and 51.8(11)%. Atomic parameters at 80 K and 16 K can be obtained as supplementary material.

atom	site	x	y	z	U_{iso}
V1	6g	0.31549(3)	0.10972(3)	0.40031(3)	0.354(7)
V2	6g	0.31643(3)	0.149623(3)	0.75026(4)	0.316(6)
V3	6g	0.31391(3)	0.18514(3)	0.10094(3)	0.390(7)
Na1	1a	0	0	0	0.8(1)
Na2	1b	0	0	0.5	1.2(1)
Na3	2d	$\frac{1}{3}$	$\frac{2}{3}$	0.0701(1)	0.79(2)
Na4	2d	$\frac{1}{3}$	$\frac{2}{3}$	0.4332(1)	0.95(2)
Na5	6g	0.5074(1)	0.4805(1)	0.2492(1)	2.07(2)
O1	6g	0.4780(1)	0.1491(2)	0.4380(1)	1.02(2)
O2	6g	0.4889(1)	0.2194(1)	0.7517(2)	1.02(3)
O3	6g	0.4760(2)	0.3083(2)	0.0636(1)	1.15(3)
O4	6g	0.2475(1)	0.9508(1)	0.7091(1)	0.59(2)
O5	6g	0.2432(2)	0.0664(1)	0.9329(1)	0.65(2)
O6	6g	0.2526(1)	0.1701(2)	0.5668(1)	0.67(2)
O7	6g	0.2715(1)	0.2987(1)	0.7911(1)	0.52(2)

TABLE III: Anisotropic displacement parameters U_{ij} (10\AA^2) in $\text{Na}_2\text{V}_3\text{O}_7$ at 200 K.

atom	U_{11}	U_{22}	U_{33}	U_{23}	U_{13}	U_{12}
V1	0.36(1)	0.40(1)	0.30(1)	-0.044(9)	-0.07(1)	0.19(1)
V2	0.28(1)	0.39(1)	0.25(1)	-0.023(9)	-0.02(1)	0.15(1)
V3	0.42(1)	0.46(1)	0.31(1)	0.011(9)	0.06(1)	0.23(1)
Na1	0.7(2)	0.7(2)	1.2(2)	0	0	0.34(8)
Na2	1.1(1)	1.1(1)	1.7(2)	0	0	0.54(7)
Na3	0.79(3)	0.79(3)	0.80(6)	0	0	0.39(2)
Na4	1.00(3)	1.00(3)	0.87(6)	0	0	0.50(2)
Na5	1.16(4)	1.56(4)	2.51(4)	-0.40(3)	-0.52(3)	-0.05(3)
O1	0.69(6)	1.39(7)	1.08(6)	-0.42(5)	-0.25(5)	0.58(5)
O2	0.54(6)	1.30(7)	0.89(5)	-0.12(5)	-0.03(5)	0.22(5)
O3	0.69(6)	1.31(7)	1.11(6)	-0.16(5)	0.16(5)	0.25(5)
O4	0.80(5)	0.41(5)	0.34(5)	-0.04(4)	0.03(4)	0.14(5)
O5	0.99(6)	0.48(6)	0.38(6)	-0.04(4)	0.11(4)	0.31(5)
O6	1.23(6)	0.77(6)	0.33(6)	-0.04(4)	0.04(5)	0.74(6)
O7	0.65(5)	0.67(6)	0.38(5)	-0.02(4)	0.02(4)	0.43(5)

TABLE IV: Shortest V-V distances (\AA) at 200 K, 80 K, 16 K and difference d between the values at 16 K and 200 K. The notations of Figure 2d are used.

V-V distance	200 K	80 K	16 K	d
1 st intra-ring				
11-31	2.9770(4)	2.9648(4)	2.955(1)	-0.022(1)
21-32	2.9851(4)	2.9908(4)	2.996(1)	+0.011(1)
11-21	2.9917(5)	2.9976(4)	3.001(1)	+0.010(1)
2 nd intra-ring				
21-31	3.6109(4)	3.6008(4)	3.596(1)	-0.015(1)
11-22	3.6588(5)	3.6635(4)	3.663(1)	+0.004(1)
1 st inter-ring				
11-23	3.3696(5)	3.3670(4)	3.365(1)	-0.004(1)
24-31	3.3732(5)	3.3716(4)	3.369(1)	-0.005(1)
2 nd inter-ring				
31-33	3.5447(4)	3.5436(4)	3.545(1)	0.000(1)
11-12	3.5694(5)	3.5760(4)	3.578(1)	+0.009(1)

TABLE V: V-O-V angles (deg) at 200 K, 80 K, 16 K associated with the shortest V-V distances. The notations of Figure 2d are used.

V-O-V angle	200 K	80 K	16 K
1 st intra-ring			
11-O 7-31	98.01(6)	97.28(5)	97.1(1)
11-O 4-31	99.56(6)	99.26(5)	98.9(1)
21-O 4-32	99.13(6)	99.55(5)	99.9(1)
21-O 5-32	101.31(6)	101.39(6)	101.4(2)
11-O 7-21	98.19(5)	98.24(5)	98.4(1)
11-O 6-21	101.86(6)	102.07(6)	102.3(2)
2 nd intra-ring			
21-O 7-31	136.15(7)	135.41(7)	135.2(2))
11-O 4-22	142.50(7)	143.41(7)	143.9(2)
1 st inter-ring			
11-O 6-23	119.16(7)	119.02(7)	119.0(2)
24-O 5-31	119.56(7)	119.48(6)	119.3(2)
2 nd inter-ring			
31-O 5-33	132.20(7)	132.00(7)	132.0(2)
11-O 6-12	133.49(7)	133.61(7)	133.5(2)

could not be avoided. However it contains nonmagnetic V^{5+} and does not affect our findings on the magnetic properties of $\text{Na}_2\text{V}_3\text{O}_7$.

147, 676 (1999).

² J. L. Gavilano, D. Rau, S. M. Ushakov, H. R. Ott, P. Millet, F. M. Ilia, Phys. Rev. Lett. 90, 167202 (2003).

³ J. L. Gavilano, E. Felder, D. Rau, H. R. Ott, P. Millet, F. M. Ilia, T. Cichorek, A. C. Mota, Phys. Rev. B 72, 64431 (2005).

⁴ M.-H. Whangbo and H.-J. Koo Solid State Comm. 115, 675 (2000).

⁵ T. Saha-Dasgupta, R. Valent, F. Capraro, C. Gros, Phys. Rev. Lett. 95, 107201 (2005).

⁶ V. V. Mazurenko, F. M. Ilia, V. I. Anisimov, Phys. Rev. B 73, 14418 (2006).

⁷ S. Naitaka, K. Yoshimura, A. Ikawa, K. Kosuge, J. Phys. Soc. Jpn 71, 208 (2002) Suppl.

⁸ The sample was stored in He atmosphere as it was unstable in air. Unfortunately a small amount of impurity NaVO_3

⁹ G. M. Sheldrick SHELX97 and SHELXL97. Programs for the solution and refinement of crystal structures; University of Göttingen: Göttingen, Germany, 1997.

¹⁰ J. Rodriguez-Carvajal, Physica 192B, 55 (1993).

¹¹ J. R. Stewart, P. P. Deen, K. H. Andersen, H. Schöber, J. F. Barthelmy, J. H. Hillier, A. P. Murari, T. Hayes, B. Lindenau and P. Hoghoj, J. Appl. Cryst. to be published.

¹² T. Vertesi, E. Bene, Phys. Rev. B 73, 134404 (2006).

¹³ O. Scharpf, H. Capellmann, Phys. Stat. Sol. (a) 135, 359 (1993).

¹⁴ A. Furrer, H. U. Gudel, J. Magn. Mater. 14, 256 (1979).

¹⁵ H. Weihe, Department of Chemistry, University of Copenhagen, Denmark.

¹⁶ The lattice contribution C_{lat} was estimated using the De-

- bye model with $T_D = 125$ K (the contribution from the optical modes is negligible in our experiments).
- ¹⁷ J. Choi, J. L. Musfeldt, Y. J. Wang, H.-J. Koo, M.-H. Whangbo, J. Galy, P. Millet, *Chem. Mater.* **14**, 924 (2002).
 - ¹⁸ N. E. Phillips, *CRC Critical Reviews in Solid State Sciences*, p 467 (1971).
 - ¹⁹ In "NMR properties of Selected Isotopes", p. 10, Bunker A. Macnicol, 2007.
 - ²⁰ T. Ohama, H. Yasuoka, M. Isobe and Y. Ueda, *Phys. Rev. B* **59**, 3299 (1999).
 - ²¹ Spin glasses, edited by K. H. Fischer and J. A. Hertz (Cambridge University Press, Cambridge, England, 1991); J. A. Mydosh *Spin glasses: An Experimental Introduction* (Taylor and Francis, London, 1993).
 - ²² J. L. van Hemmen, A. Suto, *Z. Phys. B - Condensed Matter* **61**, 263 (1985).
 - ²³ J. L. van Hemmen, G. J. Nieuwenhuys, *Europhys. Lett.* **2**, 797 (1986).
 - ²⁴ F. Luis, J. Bartolomé, J. F. Fernández, J. Tejada, J. M. Hernández, X. X. Zhang, R. Zib, *Phys. Rev. B* **55**, 11448 (1997).
 - ²⁵ I. Chiorescu, W. Wemdsorfer, A. Müller, S. Miyashita, B. Barbara, *Phys. Rev. B* **67**, 020402(R) (2003).
 - ²⁶ J. van Slageren, P. Rosa, A. Caneschi, R. Sessoli, H. Casel-
 - las, Y. V. Rakitin, L. Cianchi, F. DelGiablo, G. Spina, A. Bino, A.-L. Barra, T. Guidi, S. Carretta, and R. Cacioppo, *Phys. Rev. B* **73**, 014422 (2006).
 - ²⁷ K. I. Kugel and D. I. Khomskii, *Sov. Phys. Usp.* **25**, 231 (1982).
 - ²⁸ J. J. Borrás-Alm enar, J. M. Clemente-Juan, E. Coronado, B. S. T. Sukerblat *Inorg. Chem.* **38** (1999) 6081.
 - ²⁹ J. Schnack, H. Nojiri, P. Kogerler, G. J. T. Cooper, L. Cronin, *Phys. Rev. B* **70**, 174420 (2004).
 - ³⁰ M. Johansson K. W. Tomroos, F. Mila, P. Millet, *Chem. Mater.* **12**, 2853 (2000).
 - ³¹ O. Zaharko, A. Daoud-Aladine, S. Streule, J. Mesot, P. J. Brown, and H. Berger, *Phys. Rev. Lett.* **93**, 217206 (2004).
 - ³² A. Luscher, R. M. Noack, G. Misguich, V. N. Kotov, F. Mila, *Phys. Rev. B* **70**, 060405(R) (2004).
 - ³³ A. F. Albuquerque, F. Alet, P. Corboz, P. Dayal, A. Feiguin, S. Fuchs, L. Gamper, E. Gull, S. Guertler, A. Honecker, R. Igarashi, M. Koerner, A. Kozhevnikov, A. Laeuchli, S. Ranm ana, M. Matsumoto, I. P. McCulloch, F. Michel, R. M. Noack, G. Pawłowski, L. Pollet, T. Pruschke, U. Schollwöck, S. Todo, S. Trebst, M. Troyer, P. Werner, S. Wessel, J. von M. and M. M. Materials **310**, 1187 (2007).